Available online at www.sciencedirect.com
ScienceDirect
Journal of Power Sources 158 (2006) 1405–1409
JOURNAL OF POWER SOURCES
www.elsevier.com/locate/jpowsour

Short communication

Synthesis and characterizations of $Li[Cr_xLi_{(1-x)/3}Mn_{2(1-x)/3}]O_2$ $(0.15 \leq x \leq 0.3)$ cathode materials in rechargeable lithium batteries

I. Ruth Mangani, C.W. Park, S.H. Kim, J. Kim *

Department of Materials Science and Engineering, Chonnam National University, Gwangju 500 757, South Korea

Received 25 September 2005; received in revised form 10 October 2005; accepted 10 October 2005
Available online 14 November 2005

Abstract

A series of $Li[Cr_xLi_{(1-x)/3}Mn_{2(1-x)/3}]O_2$ $(0.15 \leq x \leq 0.3)$ cathode materials was prepared by citric acid-assisted, sol–gel process. Sub-micron sized particles were obtained and the X-ray diffraction (XRD) results showed that the crystal structure was similar to layered lithium transition metal oxides (R-3m space group). The electrochemical performance of the cathodes was evaluated over the voltage range 2.0–4.9 V at a current density of 7.947 mA g^{-1}. The $Li_{1.27}Cr_{0.2}Mn_{0.53}O_2$ electrode delivered a high reversible capacity of up to 280 mAh g^{-1} during cycling. $Li[Cr_xLi_{(1-x)/3}Mn_{2(1-x)/3}]O_2$ yielded a promising cathode material.

Keywords: Lithium batteries; Cathode materials; Layered compound; Transition metal oxides; Sol–gel process

1. Introduction

Advances in electrode materials have played a critical role in the development of rechargeable lithium-ion batteries. Several compounds, such as spinel $LiMn_2O_4$, layered $LiCoO_2$ and $LiNiO_2$, have been widely investigated [1–3]. The layered $LiMnO_2$ material is also of interest as a cathode material due to the cost effective and non-toxic properties of manganese-based materials. However, the capacity of the layered $LiMnO_2$ experiences severe decline due to the structural transition into spinel during cycling. This capacity fade renders the material undesirable for practical applications [4].

To improve the capacity during cycling, stabilization of the layered structure was considered to be essential. The structural instability arises from the weak bonding between manganese on octahedral sites and the surrounding six oxygen atoms. Hence, it was thought that the Mn^{2+} produced by the disproportionated Mn^{3+} diffuses through tetrahedral sites into the lithium layer [5]. Attempts have been made to stabilize the layered structure by partially substituting manganese with other transition metal ions [6]. Chromium-substituted, layered manganese oxide cathodes have been studied by many research groups [7,8]. Substitution of chromium in manganese sites produces structural modifications, which depend on the chromium concentration and processing temperatures [9]. Recently, a new series of compounds with the chemical formula $Li[Cr_xLi_{(1-x)/3}Mn_{2(1-x)/3}]O_2$ have been developed and they show high capacity and good retention of capacity during cycling [10,11].

In view of this, the main objective of the present work was to prepare a series of materials $Li[Cr_xLi_{(1-x)/3}Mn_{2(1-x)/3}]O_2$ $(0.15 \leq x \leq 0.3)$ by a citric acid-assisted, sol–gel method and to study the electrochemical performance.

2. Experimental

2.1. Synthesis of $Li[Cr_x\ Li_{(1-x)/3}Mn_{2(1-x)/3}]O_2$ $(0.15 \leq x \leq 0.3)$ using the sol–gel technique

Cathode materials were prepared by the sol–gel method using citric acid as the chelating agent. Aqueous solutions of lithium, manganese and chromium acetates were taken in stoichiometric amounts and dissolved in deionized water. Citric acid was added to this mixed solution in the desired proportion. The pH of the mixed solution was maintained between 6.5 and 7 with ammonium hydroxide solution. The solution was stirred for 24 h to ensure that the reaction reagents were uniformly mixed and that the complex reaction between Mn^{3+} and citric acid was

* Corresponding author. Tel.: +82 625 301 703; fax: +82 625 301 699.
E-mail address: jaekook@chonnam.ac.kr (J. Kim).

0378-7753/$ – see front matter © 2005 Elsevier B.V. All rights reserved.
doi:10.1016/j.jpowsour.2005.10.015

completed. The precipitate of metal citrate was dried in a vacuum oven for 10 h at 100 °C to give a porous, foam-like substance. In order to eliminate the organic contents, the gel precursor was calcined at 300 °C for about 10 h. The resulting powder was ground well in an agate mortar and heated at 950 °C for 12 h and then quenched.

2.2. Instrumentation

Thermal gravimetric analysis (TGA/DTA) of the precursor powder was done on an SDT Q600 V8.0 Build 95 thermal analyzer at a heating rate of 10 °C min^{-1} from room temperature to 900 °C in air. The powders were identified by X-ray diffraction (XRD) using a D/MAX Ultima III (Rigaku, Japan), with Cu Kα radiation (λ = 1.54056 Å). The lattice parameters were derived using the Rietveld method. The morphology of the samples was examined by scanning electron microscopy (SEM) (JSM, 5400-JEOL). The elemental composition of the prepared cathode powders was determined by inductively coupled plasma (ICP), using a Perkin Elmer 4300 DV analyzer.

The electrochemical performance of the prepared cathode materials was determined in galvanostatic cycling experiments. The test cells were assembled in an argon atmosphere. The electrolyte consisted of 1 M $LiPF_6$ with ethylene carbonate and diethyl carbonate. The cathode materials were mixed with carbon and binder in the appropriate weight ratio of (85:10:5).

3. Results and discussion

3.1.1. Thermal analysis

Fig. 1 shows the TG/DTA curves of $Li[Cr_xLi_{(1-x)/3}Mn_{2(1-x)/3}]O_2$ ($0.15 \le x \le 0.3$), as prepared by the citric acid-assisted, sol–gel method, and the indicates the formation of a layered phase of the precursor materials. There was a small weight loss over the temperature range 180–200 °C, which was attributed to the emission of residual water molecules and some gases adsorbed during the formation of the cathode gel precursor. The exothermic peak of lower intensity at around 220–230 °C indicates the process of decomposition of the organic components. This was followed by a very strong and vigorous reaction accompanied by a considerable weight loss due to the combustible organic materials. A weight loss observed in the TGA curve over the temperature range 280–400 °C was indicated by the sharp and narrow exothermic peak initiating around 280 °C and continuing to around 400 °C. This phenomenon may be ascribed to the decomposition of the remaining organic elements. It is apparent that the formation temperature of the layered phase commenced at around 280 °C and increased with increasing chromium content in the samples. The absence of any heat and weight transformation on the TG curve at higher temperatures indicated the completion of the decomposition of unwanted organic elements and, therefore, the formation of a well-layered phase.

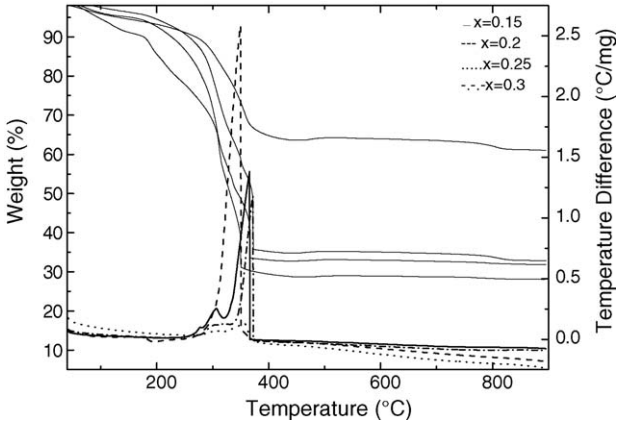

Fig. 1. TG/DTA curves of $Li[Cr_xLi_{(1-x)/3}Mn_{2(1-x)/3}]O_2$ ($0.15 \le x \le 0.3$) powder prepared by the sol–gel method.

3.1.2. Structure analysis

Fig. 2 shows the XRD pattern of the $Li[Cr_xLi_{(1-x)/3}Mn_{2(1-x)/3}]O_2$ ($0.15 \le x \le 0.3$) prepared by the sol–gel technique. A single phase $Li[Cr_xLi_{(1-x)/3}Mn_{2(1-x)/3}]O_2$ ($0.15 \le x \le 0.3$), with an α-$NaFeO_2$ type structure, was grown when the precursor was quenched at 900 °C. The XRD peaks were indexed in the hexagonal system assuming (R-3m) symmetry. In addition, there were two super-lattice ordering peaks between 20 and 30° which resulted from the short-range ordering of the lithium, chromium and manganese atoms in the transition metal layers [12]. It was assumed that the lithium ions were located in the octahedral sites between the ($Cr:Mn:O_2$) infinite slabs formed by edge sharing.

The unit cell parameters of $Li[Cr_xLi_{(1-x)/3}Mn_{2(1-x)/3}]O_2$ ($0.15 \le x \le 0.3$) were calculated using the Rietveld refinement of the XRD pattern with an (R-3m) structural model and the FULL-PROF program [13]. The unit cell parameters for the hexagonal cell are tabulated in Table 1. The unit cell parameters linearly increased with increasing x in $Li[Cr_xLi_{(1-x)/3}Mn_{2(1-x)/3}]O_2$. The variation of the lattice parameters with x content is shown in Fig. 3. These results are in good agreement with the reported

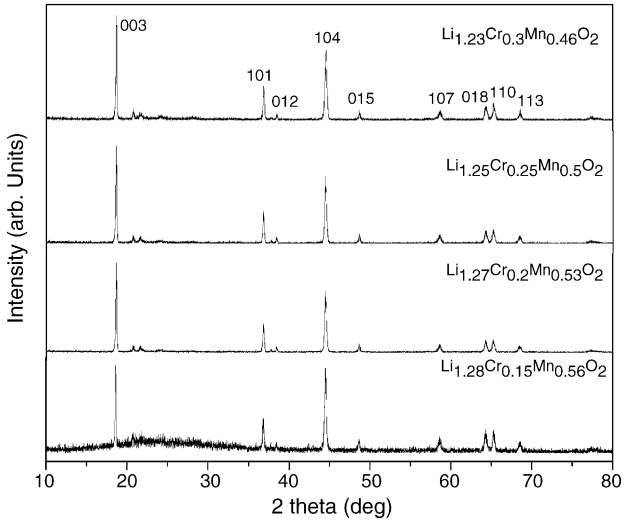

Fig. 2. XRD pattern of the $Li[Cr_xLi_{(1-x)/3}Mn_{2(1-x)/3}]O_2$ ($0.15 \le x \le 0.3$) powders prepared by sol–gel technique.

Table 1
Unit cell parameters of $Li[Cr_xLi_{(1-x)/3}Mn_{2(1-x)/3}]O_2$, $(0.15 \le x \le 0.3)$ cathode materials

Compounds	Lattice parameter (Å)		Trigonal distortion (*c*/*a*)
	a	*c*	
$Li_{1.28}Cr_{0.15}Mn_{0.56}O_2$	2.8600	14.2573	4.985
$Li_{1.27}Cr_{0.2}Mn_{0.53}O_2$	2.8649	14.2586	4.996
$Li_{1.25}Cr_{0.25}Mn_{0.50}O_2$	2.8655	14.2632	4.977
$Li_{1.23}Cr_{0.3}Mn_{0.46}O_2$	2.8653	14.2629	4.977

values [10]. The increase in the lattice parameter was attributed to the substitution of the larger Cr^{3+} (radius = 0.615 Å) ion for Mn^{4+} (radius = 0.53 Å) ion. It has been reported that a *c*/*a* ratio of 4.90 corresponds to cubic lattice constants [9]. With increased *c*/*a* ratio deviation from 4.90, the layered character improves and becomes more hexagonal-shaped. The ratio of the intensities of the (0 0 3) and (1 0 4) peaks are greater than unity which suggested the absence of any cation disorder, as was clearly observed with the *c*/*a* values. In the present study, the $Li[Cr_xLi_{(1-x)/3}Mn_{2(1-x)/3}]O_2$ $(0.15 \le x \le 0.3)$ samples had a *c*/*a* ratio around 4.97, from which we concluded that the prepared samples had a pronounced layered structure. From the Rietveld refinement XRD pattern of $Li_{1.27}Cr_{0.2}Mn_{0.53}O_2$, as shown in Fig. 4, it is very clear that the presence of the superstructure peaks in the region 20–30° resulted from the ordering of lithium and manganese in the transition metal layers.

The stoichiometry of the synthesized cathode material was confirmed by ICP-AES analysis. The chemical composition as determined from the ICP analysis was found to be close to the stoichiometry of the prepared powder.

Surface morphology and texture, as well as particle sizes, were observed by SEM. Fig. 5 shows the SEM images of $Li[Cr_xLi_{(1-x)/3}Mn_{2(1-x)/3}]O_2$ $(0.15 \le x \le 0.3)$ prepared by the sol–gel method and shows that the cathode materials had almost spherical morphology, the particles were non-agglomerated and the particle size was decreased with increasing chromium content. The particle size is found to be 4.3, 2.7, 2 and 1.7 μm,

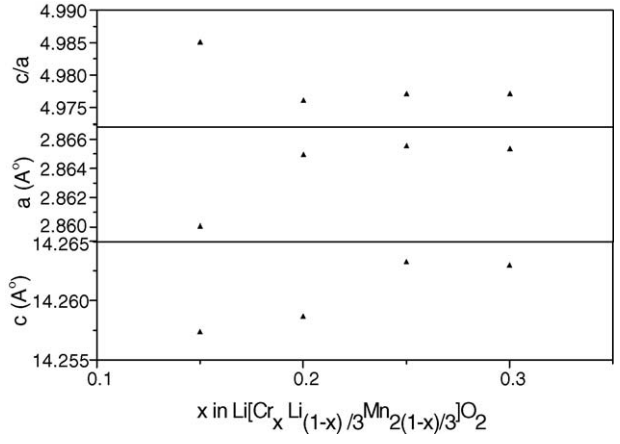

Fig. 3. Variation of the unit cell parameters with *x* content in $Li[Cr_xLi_{(1-x)/3}Mn_{2(1-x)/3}]O_2$ $(0.15 \le x \le 0.3)$.

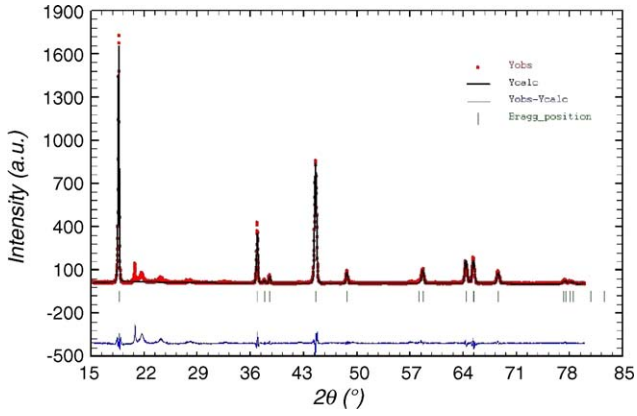

Fig. 4. Rietveld refinements to the diffraction pattern of $Li_{1.27}Cr_{0.2}Mn_{0.53}O_2$. The calculated patterns are based on the $LiMnO_2$ structure.

respectively for $x = 0.15$, 0.2, 0.25 and 0.3. The samples prepared by the sol–gel route were not hygroscopic, as were those prepared by the solution method.

3.1.3. Electrochemical performance

The first few discharge curves of the $Li[Cr_xLi_{(1-x)/3}Mn_{2(1-x)/3}]O_2$ $(0.15 \le x \le 0.3)$ cathode material are presented in Fig. 6. Test cells were operated over the voltage range 2.0–4.9 V with a current density of 10 mA g^{-1}. The figure shows that the initial discharge capacity was increased with increasing chromium content. It is believed that at the end of the first charging, when all the lithium had been extracted from the structure, the manganese ions were in the (4+) oxidation state and since these Mn^{4+} ions cannot be oxidized beyond (4+), it is assumed that Mn^{4+} does not take part in the redox reaction [4]. It has been reported that the Cr^{3+} in $Li[Cr_xLi_{(1-x)/3}Mn_{2(1-x)/3}]O_2$ is oxidized to Cr^{6+} and simultaneously moves from the original octahedral sites in the transition metal layer to neighboring tetrahedral sites in the lithium layer [14]. Upon discharge, only a certain number of chromium atoms return to their octahedral sites in the transition metal layer and the remaining chromium atoms exist on both the tetrahedral and the octahedral sites in the lithium layer. These residual transition metal atoms induce structural ordering and a large irreversible capacity on the first cycle [14].

The $Li//Li_{1.28}Cr_{0.15}Mn_{0.56}O_2$ cell delivered an initial discharge capacity of 194 mAh g^{-1}, which gradually increased over the next few cycles. Similarly, the initial discharge capacities of $Li[Cr_xLi_{(1-x)/3}Mn_{2(1-x)/3}]O_2$ ($x = 0.2$, 0.25 and 0.3) were 207, 219 and 222, respectively. Fig. 6 shows that the discharge profile of $Li_{1.27}Cr_{0.2}Mn_{0.53}O_2$ was distinctly different from that of the other compositions. The electrochemical study concentrated on this cathode material because it has been reported that in the series of various compositions of the $Li[Cr_xLi_{(1-x)/3}Mn_{2(1-x)/3}]O_2$ cathode prepared by the solution method, the $x = 0.2$ composition delivered the highest reversible capacity of 255 mAh g^{-1} [9].

From the present investigation into the electrochemical performance of $Li_{1.27}Cr_{0.2}Mn_{0.53}O_2$ cathode prepared by sol–gel

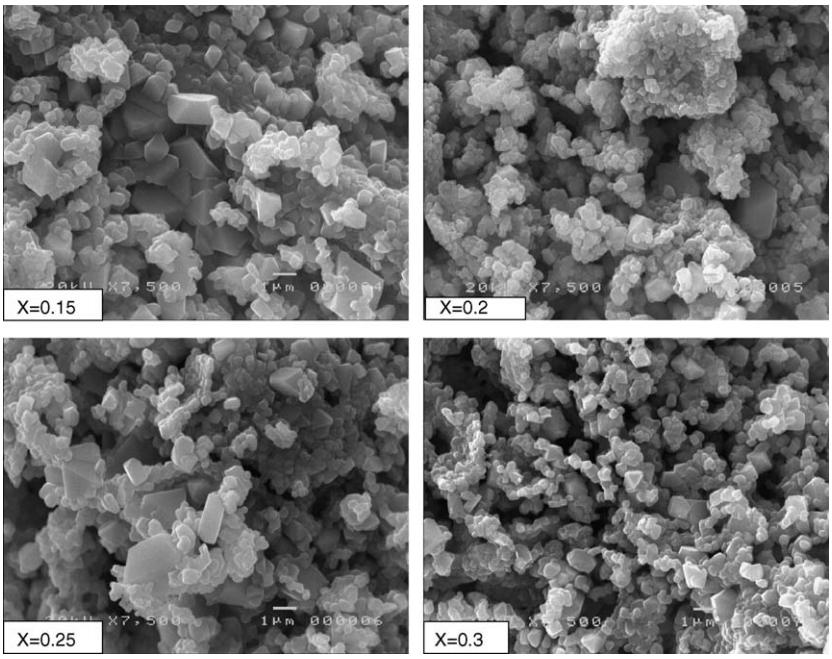

Fig. 5. SEM images of $Li[Cr_xLi_{(1-x)/3}Mn_{2(1-x)/3}]O_2$, $(0.15 \le x \le 0.3)$ powders quenched at 900 °C.

method, the discharge capacity of $Li_{1.27}Cr_{0.2}Mn_{0.53}O_2$ was found to be 280 mAh g^{-1} at the 5th cycle of discharging with the sloping voltage line increased to the upper voltage range. This capacity value may be attributed to the smaller particle size and relatively uniform distribution of particles of the cathode material, as shown by the SEM images. With continued cycling, the capacity was increased to some extent. The capacity at the 10th cycle was found to be 250 mAh g^{-1} and was stable beyond the 10th cycle. Fig. 7 shows the cycle versus capacity of the $Li_{1.27}Cr_{0.2}Mn_{0.53}O_2$ cathode material. The discharge capacity was increased to 282 mAh g^{-1} at the 5th cycle, then decreased slightly to 255 mA g^{-1} and was maintained constant beyond the 10th cycle.

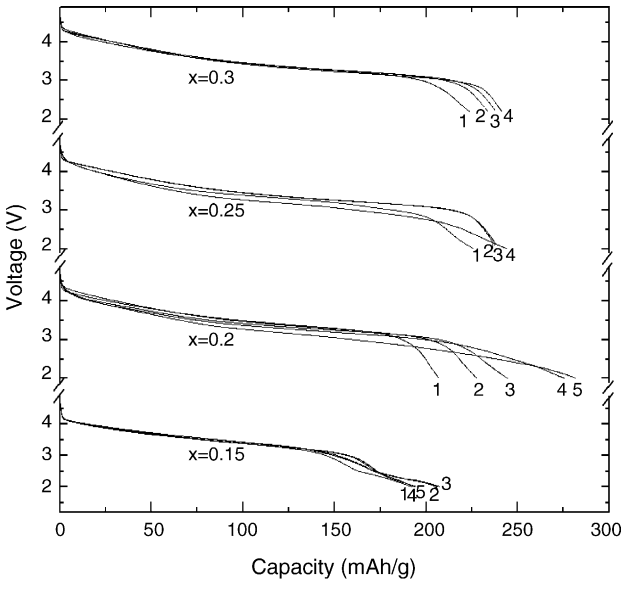

Fig. 6. Discharge profiles of $Li[Cr_xLi_{(1-x)/3}Mn_{2(1-x)/3}]O_2$, $(0.15 \le x \le 0.3)$ cathode materials cycled with a current density of 7.947 mAh g^{-1} over the voltage range 2.0–4.9 V.

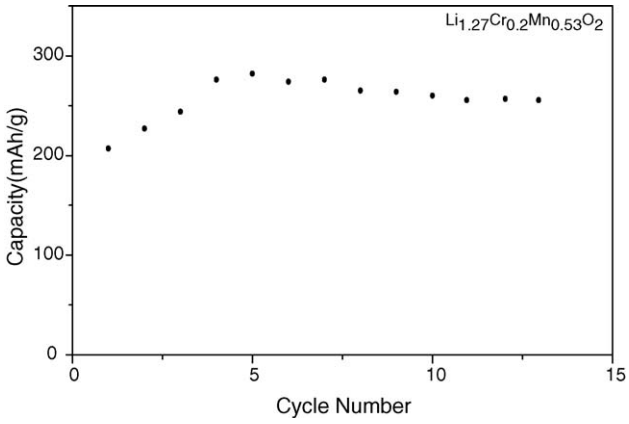

Fig. 7. Discharge capacity vs. cycle number for $Li//Li_{1.27}Cr_{0.2}Mn_{0.53}O_2$ cells cycled with a current density of 7.947 mAh g^{-1} over the voltage range 2.0–4.9 V.

4. Conclusion

A series of $Li[Cr_xLi_{(1-x)/3}Mn_{2(1-x)/3}]O_2$ $(0.15 \le x \le 0.3)$ cathode materials was prepared by the sol–gel method. The prepared materials were grown with a well-defined, layered structure. The low temperature synthesis technique adopted for the cathode materials yielded micron sized particles whose dimensions were studied for fast lithium intercalation and deintercalation reactions occurring in level mixing and highly uniform materials. The electrochemical studies also demonstrated that the $Li_{1.27}Cr_{0.2}Mn_{0.53}O_2$ cathodes yield a high capacity of about 280 mAh g^{-1} over the first few cycles. The charge–discharge profiles of the cathode materials showed evolutions which resulted from the redox reactions of the chromium ions.

Acknowledgement

This work was supported by the Core Technology Development Program of the Ministry of Commerce, Industry and Energy (MOCIE).

References

[1] J.R. Dahn, U. Von Sacken, C.A. Michal, Solid State Ionics 44 (1990) 87–97.
[2] T. Ohzuku, A. Ueda, M. Nagayama, Y. Iwakoshi, H. Komori, Electrochim. Acta 38 (1993) 1159–1167.
[3] K. Mizushima, P.C. Jones, P.J. Wiseman, J.B. Goodenough, Mater. Res. Bull. 18 (1983) 461.
[4] B. Ammundsen, J. Paulsen, Adv. Mater. 13 (2001) 943.
[5] J. Reed, G. Ceder, Chem. Rev. 104 (2004) 4513.
[6] M. Wakihara, Mater, Sci. Eng. R33 (2001) 109.
[7] J.R. Dahn, T. Zheng, C.L. Thomas, J. Electrochem. Soc. 145 (1998) 851.
[8] I.J. Davidson, R.S. Macmillan, H. Slegr, B. Luan, I. Kargina, J.J. Murray, I.P. Swainson, J. Power Sources 81 (1999) 406.
[9] B. Ammundsen, J. Paulsen, I. Davidson, R.S. Liu, C.H. Shen, J.M. Chen, L.Y. Jang, J.F. Lee, J. Electrochem. Soc. 149 (2002) A431.
[10] Z. Lu, J.R. Dahn, J. Electrochem. Soc 149 (2002) A1454.
[11] X. Wu, S.H. Chang, Y.J. Park, K.S. Ryu, J. Power Sources 137 (2004) 105.
[12] Z. Lu, J.R. Dahn, J. Electrochem. Soc. 149 (2002) A176.
[13] J. Rodriguez-Carvajal, FULLPROF: A Program for Rietveld Refinement and Pattern Matching Analysis, Abstracts of the Satellite Meeting on Powder Diffraction of the XV Congress of the IUCr, 1990, Toulouse, France, p. 127.
[14] Z. Lu, J.R. Dahn, J. Electrochem. Soc. 150 (2003) A1044.